

# Complete freezing of initially maximal entanglement in Schwarzschild black hole

Si-Han Li, Hui-Chen Yang, Rui-Yang Xu, Shu-Min Wu\*

*Department of Physics, Liaoning Normal University, Dalian 116029, China*

## Abstract

Gravitational effects associated with black holes are widely believed to universally degrade quantum entanglement, with the loss of maximal entanglement being particularly severe and even irreversible for bosonic fields. In this work, we investigate the entanglement properties of the four-qubit cluster state ( $CL_4$ ) for fermionic fields in the curved spacetime of a Schwarzschild black hole. Remarkably, we uncover a counterintuitive phenomenon: as the Hawking temperature increases, quantum entanglement (1-3 tangle) of the  $CL_4$  state remains strictly constant, indicating a “complete freezing of initially maximal entanglement”. This constitutes the first explicit example in which maximal entanglement remains perfectly preserved in a black hole environment, defying the conventional expectation that gravitational effects can only suppress maximal quantum correlations. Moreover, our results indicate that, within a relativistic framework, the  $CL_4$  state constitutes a high-quality quantum resource with potential applications in relativistic quantum information processing, and may significantly improve the performance of such protocols.

PACS numbers: 04.70.Dy, 03.65.Ud, 04.62.+v

---

\* Email: smwu@lnnu.edu.cn

## I. INTRODUCTION

Quantum information in curved spacetime lies at the intersection of quantum information theory, quantum field theory, and general relativity, aiming to reveal how gravity influences fundamental quantum resources such as entanglement and coherence, to explore methods for preserving these resources in relativistic settings, and to utilize quantum technologies for probing spacetime structure [1–62]. A central research direction in this field involves studying quantum systems within the single-mode approximation of free field models. Extensive studies have shown that quantum entanglement generally degrades under both the Unruh effect in uniformly accelerated frames and the Hawking radiation produced by black holes. This conclusion has been systematically verified for a variety of fundamental entangled states, including Bell states [1–5] as well as multipartite GHZ and W states [63–69]. For bosonic fields, such degradation is particularly severe and may even lead to irreversible entanglement degradation [1–3]. Consequently, a prevailing view has emerged that gravitational environments are intrinsically detrimental to quantum entanglement, providing strong motivation to further investigate strategies for preserving quantum resources under relativistic conditions.

As relativistic quantum information tasks become more complex, multipartite entanglement plays a crucial role in supporting advanced quantum protocols. Identifying quantum states that maintain their quantum features in extreme gravitational conditions has thus become a pressing research goal. Cluster states, particularly the four-qubit  $CL_4$  state, represent a unique and valuable class of quantum resources [70–81]. Their graph-theoretic structure forms the foundation for measurement-based quantum computation, and they possess inherent robustness against local noise in inertial frames [77–85]. This natural stability raises an important and unexplored question within the single-mode approximation: given that previous quantum states typically show monotonic entanglement degradation, can the  $CL_4$  state break this pattern? More specifically, does its unique topology provide exceptional resilience, allowing it to preserve a “complete freezing of initially maximal entanglement” even under Hawking thermal noise? Answering this question is crucial, as it challenges the prevailing notion of universal entanglement degradation in gravitational environments and could identify a robust class of quantum resources ideal for quantum technologies in strong gravitational fields.

General relativity predicts the potential existence of black holes, a prediction that has since been extensively developed in the context of black hole physics and corroborated by both indirect and

direct astronomical observations. Motivated by these advances, we systematically investigate the properties of quantum entanglement of the  $CL_4$  state in the curved spacetime of a Schwarzschild black hole. In our setup, four observers—Alice, Bob, Charlie, and David—are initially placed in an asymptotically flat region, with only David approaching the event horizon of the Schwarzschild black hole. Our analysis reveals a well-defined hierarchy of robustness determined by the topological structure of multipartite quantum states in curved spacetime. Notably, a “complete freezing of initially maximal entanglement” is observed exclusively for the  $CL_4$  state: for arbitrary Hawking temperatures, the entanglement between a symmetrically paired observer (Alice or Bob) and the remaining three-party subsystem remains strictly maximal. In contrast, for other representative multipartite entangled states, such as the  $GHZ_4$  and  $W_4$  states, the corresponding entanglement degrades monotonically as the Hawking temperature increases. To the best of our knowledge, within the single-mode approximation, this work provides the first explicit evidence of complete entanglement freezing for a multipartite quantum state in a black hole environment. These results suggest that the  $CL_4$  state exhibits intrinsic, topology-dependent robustness against Hawking-induced decoherence. Our findings not only challenge the prevailing view that maximal entanglement invariably degrades in gravitational backgrounds but also position the  $CL_4$  state as a unique and promising quantum resource for relativistic quantum information processing in strong-gravity regimes.

The paper is organized as follows. In Sec. II, we introduce the quantization of the Dirac field in the Schwarzschild black hole background. In Sec. III, we analyze the entanglement properties of the  $CL_4$  state in this background. Finally, Sec. IV concludes with a summary of our findings.

## II. QUANTIZATION OF DIRAC FIELD IN SCHWARZSCHILD SPACETIME

The metric of the Schwarzschild black hole is given by

$$ds^2 = -(1 - \frac{2M}{r})dt^2 + (1 - \frac{2M}{r})^{-1}dr^2 + r^2(d\theta^2 + \sin^2\theta d\varphi^2), \quad (1)$$

where  $r$  and  $M$  denote the radius and mass of the black hole, respectively [4]. For simplicity, we adopt natural units where  $\hbar = G = c = k = 1$ . In this spacetime, the massless Dirac equation

$[\gamma^a e_a^\mu (\partial_\mu + \Gamma_\mu)]\Phi = 0$  takes the explicit form

$$\begin{aligned} & -\frac{\gamma_0}{\sqrt{1 - \frac{2M}{r}}}\frac{\partial\Phi}{\partial t} + \gamma_1\sqrt{1 - \frac{2M}{r}}\left[\frac{\partial}{\partial r} + \frac{1}{r} + \frac{M}{2r(r - 2M)}\right]\Phi \\ & + \frac{\gamma_2}{r}\left(\frac{\partial}{\partial\theta} + \frac{\cot\theta}{2}\right)\Phi + \frac{\gamma_3}{r\sin\theta}\frac{\partial\Phi}{\partial\varphi} = 0, \end{aligned} \quad (2)$$

where  $\gamma_i$  ( $i = 0, 1, 2, 3$ ) represent the Dirac matrices [6, 12].

By solving the Dirac equation near the event horizon, one obtains a complete set of positive-frequency outgoing modes. The solutions for the regions inside and outside the event horizon are, respectively:

$$\Phi_{\mathbf{k},\text{in}}^+ \sim \phi(r)e^{i\omega u}, \quad (3)$$

$$\Phi_{\mathbf{k},\text{out}}^+ \sim \phi(r)e^{-i\omega u}, \quad (4)$$

where  $\phi(r)$  is the four-component Dirac spinor and  $u = t - r_*$  is the retarded time, with the tortoise coordinate defined as  $r_* = r + 2M \ln \frac{r-2M}{2M}$  [22]. Here,  $\mathbf{k}$  and  $\omega$  denote the wave vector and frequency, satisfying the massless dispersion relation  $|\mathbf{k}| = \omega$ . The Dirac field  $\Phi$  can be quantized by expanding it in terms of the Schwarzschild modes

$$\begin{aligned} \Phi = & \int d\mathbf{k} [\hat{a}_{\mathbf{k}}^{\text{in}}\Phi_{\mathbf{k},\text{in}}^+ + \hat{b}_{\mathbf{k}}^{\text{in}\dagger}\Phi_{\mathbf{k},\text{in}}^- \\ & + \hat{a}_{\mathbf{k}}^{\text{out}}\Phi_{\mathbf{k},\text{out}}^+ + \hat{b}_{\mathbf{k}}^{\text{out}\dagger}\Phi_{\mathbf{k},\text{out}}^-], \end{aligned} \quad (5)$$

where  $\hat{a}_{\mathbf{k}}^{\text{in}}$  and  $\hat{b}_{\mathbf{k}}^{\text{in}\dagger}$  are the fermion annihilation and antifermion creation operators inside the event horizon, while  $\hat{a}_{\mathbf{k}}^{\text{out}}$  and  $\hat{b}_{\mathbf{k}}^{\text{out}\dagger}$  are the corresponding operators for the exterior region. These operators satisfy the canonical anticommutation relations  $\{\hat{a}_{\mathbf{k}}^{\text{out}}, \hat{a}_{\mathbf{k}'}^{\text{out}\dagger}\} = \{\hat{b}_{\mathbf{k}}^{\text{in}}, \hat{b}_{\mathbf{k}'}^{\text{in}\dagger}\} = \delta_{\mathbf{k}\mathbf{k}'}$ . The Schwarzschild vacuum  $|0\rangle_S$  is defined by  $\hat{a}_{\mathbf{k}}^{\text{in}}|0\rangle_S = \hat{a}_{\mathbf{k}}^{\text{out}}|0\rangle_S = 0$ .

Following the approach proposed by Damour and Ruffini [86], a complete basis of global positive-energy modes can be constructed via analytic continuation of Eqs.(3) and (4) across the horizon. This yields the Kruskal modes:

$$\Psi_{\mathbf{k},\text{out}}^+ = e^{-2\pi M\omega}\Phi_{-\mathbf{k},\text{in}}^- + e^{2\pi M\omega}\Phi_{\mathbf{k},\text{out}}^+, \quad (6)$$

$$\Psi_{\mathbf{k},\text{in}}^+ = e^{-2\pi M\omega}\Phi_{-\mathbf{k},\text{out}}^- + e^{2\pi M\omega}\Phi_{\mathbf{k},\text{in}}^+. \quad (7)$$

Using these modes, the Dirac field is expanded in the Kruskal spacetime as

$$\begin{aligned}\Phi = & \int d\mathbf{k} [2 \cosh(4\pi M\omega)]^{-\frac{1}{2}} [\hat{c}_{\mathbf{k}}^{\text{in}} \Psi_{\mathbf{k},\text{in}}^+ + \hat{d}_{\mathbf{k}}^{\text{in}\dagger} \Psi_{\mathbf{k},\text{in}}^- \\ & + \hat{c}_{\mathbf{k}}^{\text{out}} \Psi_{\mathbf{k},\text{out}}^+ + \hat{d}_{\mathbf{k}}^{\text{out}\dagger} \Psi_{\mathbf{k},\text{out}}^-],\end{aligned}\quad (8)$$

where  $\hat{c}_{\mathbf{k}}^{\sigma}$  and  $\hat{d}_{\mathbf{k}}^{\sigma\dagger}$  with  $\sigma = (\text{in}, \text{out})$  denote the annihilation and creation operators acting on the Kruskal vacuum  $|0\rangle_K$ .

Comparing the expansions in Eqs.(5) and (8) yields the Bogoliubov transformation relating the Schwarzschild and Kruskal operators [14]

$$\hat{c}_{\mathbf{k}}^{\text{out}} = \frac{1}{\sqrt{e^{-8\pi M\omega} + 1}} \hat{a}_{\mathbf{k}}^{\text{out}} - \frac{1}{\sqrt{e^{8\pi M\omega} + 1}} \hat{b}_{\mathbf{k}}^{\text{in}\dagger}, \quad (9)$$

$$\hat{c}_{\mathbf{k}}^{\text{out}\dagger} = \frac{1}{\sqrt{e^{-8\pi M\omega} + 1}} \hat{a}_{\mathbf{k}}^{\text{out}\dagger} - \frac{1}{\sqrt{e^{8\pi M\omega} + 1}} \hat{b}_{\mathbf{k}}^{\text{in}}. \quad (10)$$

Consequently, the Kruskal vacuum state  $|0\rangle_K$  and excited state  $|1\rangle_K$  can be expressed as an entangled state in the Schwarzschild Fock space

$$\begin{aligned}|0\rangle_K = & \frac{1}{\sqrt{e^{-\frac{\omega}{T}} + 1}} |0\rangle_{\text{out}} |0\rangle_{\text{in}} + \frac{1}{\sqrt{e^{\frac{\omega}{T}} + 1}} |1\rangle_{\text{out}} |1\rangle_{\text{in}}, \\ |1\rangle_K = & |1\rangle_{\text{out}} |0\rangle_{\text{in}},\end{aligned}\quad (11)$$

where  $T = \frac{1}{8\pi M}$  is the Hawking temperature. Here,  $\{|n\rangle_{\text{out}}\}$  and  $\{|n\rangle_{\text{in}}\}$  denote the Schwarzschild number states for fermions outside the event horizon and antifermions inside the event horizon, respectively [1, 66]. The Schwarzschild observer is located outside the event horizon, and its Hawking radiation spectrum is given by

$$N_F = {}_K\langle 0 | \hat{a}_{\mathbf{k}}^{\text{out}\dagger} \hat{a}_{\mathbf{k}}^{\text{out}} | 0 \rangle_K = \frac{1}{e^{\frac{\omega}{T}} + 1}. \quad (12)$$

Eq.(12) indicates that the Kruskal vacuum observed by the Schwarzschild observer would be detected as a number of generated fermions  $N_F$ . In other words, the Schwarzschild observer in the exterior of the black hole can detect a thermal bath of fermions following the Fermi-Dirac statistic.

### III. QUANTUM ENTANGLEMENT FOR THE $CL_4$ STATE IN SCHWARZSCHILD SPACETIME

In this paper, we explore the properties of quantum entanglement for tetrapartite systems in Schwarzschild spacetime. In the asymptotically flat region, the  $CL_4$  state shared by four fermionic modes is

$$|\Psi_{ABCD}^{CL_4}\rangle = \frac{1}{2} (|0_A 0_B 0_C 0_D\rangle + |0_A 0_B 1_C 1_D\rangle + |1_A 1_B 0_C 0_D\rangle - |1_A 1_B 1_C 1_D\rangle), \quad (13)$$

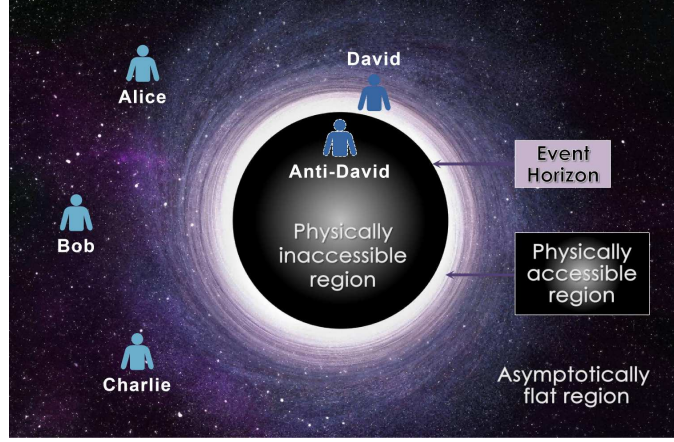


FIG. 1: Embedding diagram of the black hole and the detector configuration. Alice, Bob, Charlie and David are stationed at fixed radial positions outside the event horizon, while the anti-David mode resides in the causally inaccessible region inside the event horizon.

where the subscripts  $A$ ,  $B$ ,  $C$  and  $D$  correspond to the modes accessible to Alice, Bob, Charlie and David, respectively. To characterize the modification of this entangled state induced by the Hawking radiation, it is necessary to specify both the causal structure of the black hole spacetime and the locations of the observers. As shown in Fig.1, the black hole geometry is divided by the event horizon into two causally disconnected regions: the exterior region that extends smoothly to asymptotic flat infinity, and the interior region that cannot communicate with exterior observers. In our setup, all four observers are located outside the event horizon and couple only to exterior field modes. The partner mode inside the event horizon, denoted as anti-David and causally inaccessible to David, must be traced out to obtain the physically accessible state for the exterior observers.

Employing Eq.(11), we can rewrite Eq.(13) in terms of the Schwarzschild modes for David and its interior partner  $\bar{D}$ :

$$\begin{aligned}
 |\Psi_{ABCD\bar{D}}^{CL4}\rangle = & \frac{1}{2\sqrt{e^{-\frac{\omega}{T}} + 1}} (|0\rangle_A|0\rangle_B|0\rangle_C|0\rangle_D|0\rangle_{\bar{D}} + |1\rangle_A|1\rangle_B|0\rangle_C|0\rangle_D|0\rangle_{\bar{D}}) \\
 & + \frac{1}{2\sqrt{e^{\frac{\omega}{T}} + 1}} (|0\rangle_A|0\rangle_B|0\rangle_C|1\rangle_D|1\rangle_{\bar{D}} + |1\rangle_A|1\rangle_B|0\rangle_C|1\rangle_D|1\rangle_{\bar{D}}) \\
 & + \frac{1}{2} (|0\rangle_A|0\rangle_B|1\rangle_C|1\rangle_D|0\rangle_{\bar{D}} - |1\rangle_A|1\rangle_B|1\rangle_C|1\rangle_D|0\rangle_{\bar{D}}),
 \end{aligned} \tag{14}$$

where the mode  $\bar{D}$  is observed by a hypothetical observer (anti-David) inside the event horizon, and  $\omega$  is the frequency of the mode  $D$ . Since the exterior region of the black hole is causally disconnected from its interior, David cannot detect the physically inaccessible mode  $\bar{D}$ . Consequently,

we need to trace over this inaccessible mode to obtain the reduced density matrix describing the state of the four external observers:

$$\rho_{ABCD}^{CL_4} = \frac{1}{4} \begin{pmatrix} \frac{1}{e^{-\frac{\omega}{T}}+1} & 0 & \frac{1}{\sqrt{e^{-\frac{\omega}{T}}+1}} & \frac{1}{e^{-\frac{\omega}{T}}+1} & 0 & -\frac{1}{\sqrt{e^{-\frac{\omega}{T}}+1}} \\ 0 & \frac{1}{e^{\frac{\omega}{T}}+1} & 0 & 0 & \frac{1}{e^{\frac{\omega}{T}}+1} & 0 \\ \frac{1}{\sqrt{e^{-\frac{\omega}{T}}+1}} & 0 & 1 & \frac{1}{\sqrt{e^{-\frac{\omega}{T}}+1}} & 0 & -1 \\ \frac{1}{e^{-\frac{\omega}{T}}+1} & 0 & \frac{1}{\sqrt{e^{-\frac{\omega}{T}}+1}} & \frac{1}{e^{-\frac{\omega}{T}}+1} & 0 & -\frac{1}{\sqrt{e^{-\frac{\omega}{T}}+1}} \\ 0 & \frac{1}{e^{\frac{\omega}{T}}+1} & 0 & 0 & \frac{1}{e^{\frac{\omega}{T}}+1} & 0 \\ -\frac{1}{\sqrt{e^{-\frac{\omega}{T}}+1}} & 0 & -1 & -\frac{1}{\sqrt{e^{-\frac{\omega}{T}}+1}} & 0 & 1 \end{pmatrix}, \quad (15)$$

where the matrix is expressed in the ordered basis  $|0000\rangle$ ,  $|0001\rangle$ ,  $|0011\rangle$ ,  $|1100\rangle$ ,  $|1101\rangle$  and  $|1111\rangle$ .

To quantify the quantum entanglement between observers in this curved spacetime, we employ the negativity, a widely used entanglement measure applicable to both pure and mixed states. It is particularly effective for detecting entanglement: a bipartitioned density matrix  $\rho$  is entangled whenever its partial transpose exhibits at least one negative eigenvalue. Specifically, for a four-partite (tetrapartite) system, the negativity associated with a given bipartition is defined as

$$N_{A(BCD)} = \|\rho_{ABCD}^{T_A}\| - 1, \quad (16)$$

where  $N_{A(BCD)}$  (often referred to as the  $1 - 3$  tangle) quantifies the entanglement between a subsystem  $A$  and the remaining three subsystems  $(BCD)$ . Here,  $\|\rho_{ABCD}^{T_A}\|$  denotes the trace norm of the partially transposed density matrix. The notation  $T_A$  indicates the partial transposition with respect to subsystem  $A$  [87]. Alternatively, using the trace-norm definition  $\|O\| = \text{tr}\sqrt{O^\dagger O}$  for a Hermitian operator  $O$ , the negativity can be rewritten in a computationally more convenient form

$$\|M\| - 1 = 2 \sum_{i=1}^N |\lambda_M^{(-)}|^i, \quad (17)$$

where  $|\lambda_M^{(-)}|^i$  denotes the absolute values of the negative eigenvalues of the partially transposed matrix  $M$ . This expression provides a direct and numerically efficient way to evaluate the entanglement for a given bipartition.

We now analyze the negativity, focusing on the  $1 - 3$  tangle of the tetrapartite  $CL_4$  state described by the density matrix  $\rho_{ABCD}^{CL_4}$ . Taking the partial transpose of  $\rho_{ABCD}^{CL_4}$  with respect to sub-

system  $A$ , we obtain

$$\rho_{ABCD}^{CL_4(T_A)} = \frac{1}{4} \begin{pmatrix} \frac{1}{e^{-\frac{\omega}{T}}+1} & 0 & \frac{1}{\sqrt{e^{-\frac{\omega}{T}}+1}} & 0 & 0 & 0 & 0 & 0 & 0 & 0 & 0 & 0 \\ 0 & \frac{1}{e^{\frac{\omega}{T}}+1} & 0 & 0 & 0 & 0 & 0 & 0 & 0 & 0 & 0 & 0 \\ \frac{1}{\sqrt{e^{-\frac{\omega}{T}}+1}} & 0 & 1 & 0 & 0 & 0 & 0 & 0 & 0 & 0 & 0 & 0 \\ 0 & 0 & 0 & 0 & 0 & 0 & \frac{1}{e^{-\frac{\omega}{T}}+1} & 0 & \frac{1}{\sqrt{e^{-\frac{\omega}{T}}+1}} & 0 & 0 & 0 \\ 0 & 0 & 0 & 0 & 0 & 0 & 0 & \frac{1}{e^{\frac{\omega}{T}}+1} & 0 & 0 & 0 & 0 \\ 0 & 0 & 0 & 0 & 0 & 0 & -\frac{1}{\sqrt{e^{-\frac{\omega}{T}}+1}} & 0 & -1 & 0 & 0 & 0 \\ 0 & 0 & 0 & \frac{1}{e^{-\frac{\omega}{T}}+1} & 0 & -\frac{1}{\sqrt{e^{-\frac{\omega}{T}}+1}} & 0 & 0 & 0 & 0 & 0 & 0 \\ 0 & 0 & 0 & 0 & \frac{1}{e^{\frac{\omega}{T}}+1} & 0 & 0 & 0 & 0 & 0 & 0 & 0 \\ 0 & 0 & 0 & \frac{1}{\sqrt{e^{-\frac{\omega}{T}}+1}} & 0 & -1 & 0 & 0 & 0 & 0 & 0 & 0 \\ 0 & 0 & 0 & 0 & 0 & 0 & 0 & 0 & 0 & \frac{1}{e^{-\frac{\omega}{T}}+1} & 0 & -\frac{1}{\sqrt{e^{-\frac{\omega}{T}}+1}} \\ 0 & 0 & 0 & 0 & 0 & 0 & 0 & 0 & 0 & 0 & \frac{1}{e^{\frac{\omega}{T}}+1} & 0 \\ 0 & 0 & 0 & 0 & 0 & 0 & 0 & 0 & 0 & -\frac{1}{\sqrt{e^{-\frac{\omega}{T}}+1}} & 0 & 1 \end{pmatrix}, \quad (18)$$

where the matrix is expressed in the ordered basis  $|0000\rangle, |0001\rangle, |0011\rangle, |0100\rangle, |0101\rangle, |0111\rangle, |1000\rangle, |1001\rangle, |1011\rangle, |1100\rangle, |1101\rangle$  and  $|1111\rangle$ . Using Eq.(17) to compute the negativity, we obtain

$$N_{A(BCD)}^{CL_4} = 1, \quad (19)$$

indicating that the entanglement between subsystem  $A$  and the remaining three parties is maximal. Due to the symmetry of the  $CL_4$  state under exchange of Alice and Bob (see Eq.(13)), the same result holds for the bipartition involving Bob:  $N_{A(BCD)}^{CL_4} = N_{B(ACD)}^{CL_4}$ . Thus, the entanglement between Alice (or Bob) and the rest of the system remains strictly maximal across the entire range of Hawking temperatures, a phenomenon we refer to as the “complete freezing of initially maximal entanglement” in a strong gravitational field. This section focuses on the  $CL_4$  state, with comparative analyses of the  $GHZ_4$  and  $W_4$  states under identical conditions presented in Appendices A and B, respectively.

Fig.2 shows the negativity  $N_{A(BCD)}$  for the  $CL_4$ ,  $GHZ_4$ , and  $W_4$  states as a function of the Hawking temperature  $T$ , with a fixed mode frequency  $\omega = 1$ . A key feature of this analysis is the complete freezing of entanglement observed exclusively for the  $CL_4$  state. Specifically, its negativity  $N_{A(BCD)}^{CL_4}$  (and, by symmetry,  $N_{B(ACD)}^{CL_4}$ ) remains identically maximal ( $N_{A(BCD)}^{CL_4} = 1$ ) across the entire range of Hawking temperatures. This provides direct evidence, within the single-mode approximation, that the initial maximal entanglement of the  $CL_4$  state is perfectly preserved and remains entirely decoupled from the thermal fluctuations induced by the Hawking radiation.

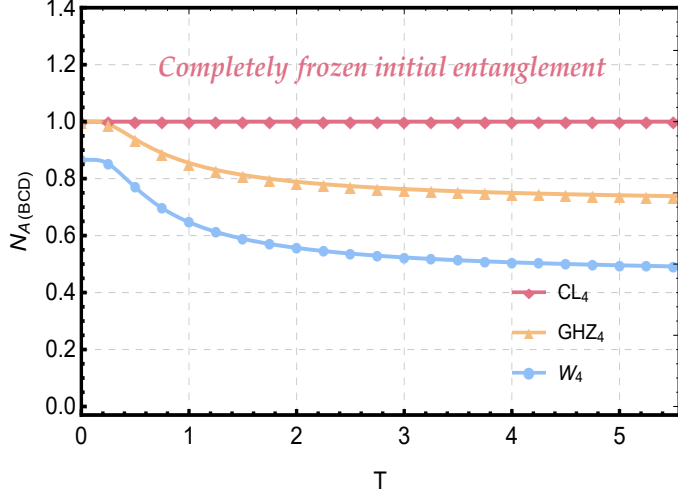


FIG. 2: The  $N_{A(BCD)}$  of the  $CL_4$ ,  $GHZ_4$  and  $W_4$  states as a function of the Hawking temperature  $T$  for a fixed mode frequency  $\omega = 1$ .

In stark contrast, the negativities of both the  $GHZ_4$  and  $W_4$  states decay monotonically with increasing temperature  $T$ , eventually approaching finite, non-zero asymptotic values. This universal degradation highlights the generic vulnerability of quantum correlations to Hawking radiation. Therefore, the persistent maximal entanglement of the  $CL_4$  state is not a generic property of multipartite systems but rather a distinctive feature arising from its specific graph-theoretic (cluster) architecture. This architecture intrinsically decouples certain bipartitions from thermal noise, offering resilience against decoherence. Our findings thus challenge the prevailing paradigm within the single-mode approximation, which suggests that Hawking radiation inevitably diminishes initially maximal quantum correlations.

We now compute the entanglement for the remaining  $1 - 3$  bipartitions by taking the partial transpose with respect to modes  $C$  and  $D$ . The resulting partially transposed density matrices can

be expressed as

$$\rho_{ABCD}^{CL_4(T_C)} = \frac{1}{4} \begin{pmatrix} \frac{1}{e^{-\frac{\omega}{T}}+1} & 0 & 0 & 0 & \frac{1}{e^{-\frac{\omega}{T}}+1} & 0 & 0 & 0 \\ 0 & \frac{1}{e^{\frac{\omega}{T}}+1} & \frac{1}{\sqrt{e^{-\frac{\omega}{T}}+1}} & 0 & 0 & \frac{1}{e^{\frac{\omega}{T}}+1} & \frac{1}{\sqrt{e^{-\frac{\omega}{T}}+1}} & 0 \\ 0 & \frac{1}{\sqrt{e^{-\frac{\omega}{T}}+1}} & 0 & 0 & 0 & -\frac{1}{\sqrt{e^{-\frac{\omega}{T}}+1}} & 0 & 0 \\ 0 & 0 & 0 & 1 & 0 & 0 & 0 & -1 \\ \frac{1}{e^{-\frac{\omega}{T}}+1} & 0 & 0 & 0 & \frac{1}{e^{-\frac{\omega}{T}}+1} & 0 & 0 & 0 \\ 0 & \frac{1}{e^{\frac{\omega}{T}}+1} & -\frac{1}{\sqrt{e^{-\frac{\omega}{T}}+1}} & 0 & 0 & \frac{1}{e^{\frac{\omega}{T}}+1} & -\frac{1}{\sqrt{e^{-\frac{\omega}{T}}+1}} & 0 \\ 0 & \frac{1}{\sqrt{e^{-\frac{\omega}{T}}+1}} & 0 & 0 & 0 & -\frac{1}{\sqrt{e^{-\frac{\omega}{T}}+1}} & 0 & 0 \\ 0 & 0 & 0 & -1 & 0 & 0 & 0 & 1 \end{pmatrix}, \quad (20)$$

$$\rho_{ABCD}^{CL_4(T_D)} = \frac{1}{4} \begin{pmatrix} \frac{1}{e^{-\frac{\omega}{T}}+1} & 0 & 0 & 0 & \frac{1}{e^{-\frac{\omega}{T}}+1} & 0 & 0 & 0 \\ 0 & \frac{1}{e^{\frac{\omega}{T}}+1} & \frac{1}{\sqrt{e^{-\frac{\omega}{T}}+1}} & 0 & 0 & \frac{1}{e^{\frac{\omega}{T}}+1} & -\frac{1}{\sqrt{e^{-\frac{\omega}{T}}+1}} & 0 \\ 0 & \frac{1}{\sqrt{e^{-\frac{\omega}{T}}+1}} & 0 & 0 & 0 & \frac{1}{\sqrt{e^{-\frac{\omega}{T}}+1}} & 0 & 0 \\ 0 & 0 & 0 & 1 & 0 & 0 & 0 & -1 \\ \frac{1}{e^{-\frac{\omega}{T}}+1} & 0 & 0 & 0 & \frac{1}{e^{-\frac{\omega}{T}}+1} & 0 & 0 & 0 \\ 0 & \frac{1}{e^{\frac{\omega}{T}}+1} & \frac{1}{\sqrt{e^{-\frac{\omega}{T}}+1}} & 0 & 0 & \frac{1}{e^{\frac{\omega}{T}}+1} & -\frac{1}{\sqrt{e^{-\frac{\omega}{T}}+1}} & 0 \\ 0 & -\frac{1}{\sqrt{e^{-\frac{\omega}{T}}+1}} & 0 & 0 & 0 & -\frac{1}{\sqrt{e^{-\frac{\omega}{T}}+1}} & 0 & 0 \\ 0 & 0 & 0 & -1 & 0 & 0 & 0 & 1 \end{pmatrix}, \quad (21)$$

where the matrix  $\rho_{ABCD}^{CL_4(T_C)}$  is expressed in the ordered basis  $|0000\rangle, |0001\rangle, |0010\rangle, |0011\rangle, |1100\rangle, |1101\rangle, |1110\rangle$  and  $|1111\rangle$ , and the matrix  $\rho_{ABCD}^{CL_4(T_D)}$  is expressed in the ordered basis  $|0000\rangle, |0001\rangle, |0010\rangle, |0011\rangle, |1100\rangle, |1101\rangle, |1110\rangle$  and  $|1111\rangle$ . Applying Eq.(17), the corresponding negativities can be expressed as

$$N_{C(ABD)}^{CL_4} = \max \left\{ 0, \frac{1}{\sqrt{1 + e^{-\frac{\omega}{T}}}} \right\}, \quad (22)$$

$$N_{D(ABC)}^{CL_4} = \max \left\{ 0, \frac{1}{2} \left( \sqrt{\frac{4}{1 + e^{-\frac{\omega}{T}}} + \frac{1}{(1 + e^{\frac{\omega}{T}})^2}} - \frac{1}{1 + e^{\frac{\omega}{T}}} \right) \right\}. \quad (23)$$

Fig.3 plots the negativities  $N_{C(ABD)}$  and  $N_{D(ABC)}$  for the  $CL_4$ ,  $GHZ_4$ , and  $W_4$  states as a function of the Hawking temperature  $T$ . A notable observation is that both the  $CL_4$  and  $GHZ_4$

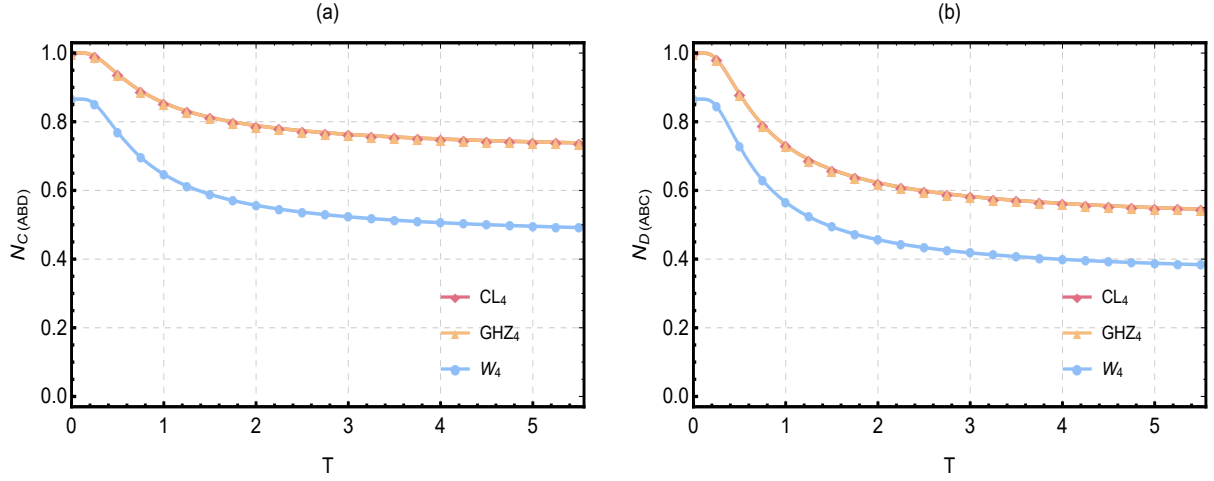


FIG. 3: The  $N_{C(ABD)}$  and  $N_{D(ABC)}$  of the  $CL_4$ ,  $GHZ_4$  and  $W_4$  states as a function of the Hawking temperature  $T$  for a fixed mode frequency  $\omega = 1$ .

states exhibit identical decay curves for both  $N_{C(ABD)}$  [Fig.3(a)] and  $N_{D(ABC)}$  [Fig.3(b)]. In all cases, the negativities decay monotonically as the Hawking temperature increases, but none of them experiences sudden entanglement death. Instead, each negativity approaches a distinct finite asymptotic value as the Hawking temperature tends to infinity ( $T \rightarrow \infty$ ). The data reveal two key hierarchies of robustness. First, for each state, the relation  $N_{C(ABD)} > N_{D(ABC)}$  holds for all values of the Hawking temperature. This indicates that the quantum entanglement measured for the mode directly exposed to the thermal bath (i.e., the mode associated with observer  $D$ ) is smaller than that measured for modes located in the asymptotically flat region. Therefore, when these modes are treated as part of the environment rather than as subsystems whose entanglement is being measured, the system exhibits a systematic robustness advantage in its entanglement properties. Second, across all three states, the  $W_4$  state consistently exhibits the lowest entanglement, with its decay curve lying below the overlapping curves of the  $CL_4$  and  $GHZ_4$  states. This observation highlights the fact that the  $W_4$  state is generally more susceptible to decoherence and thermal fluctuations than both the  $CL_4$  and  $GHZ_4$  states. This comparative analysis provides an important insight: although the  $CL_4$  state demonstrates the unique phenomenon of complete entanglement freezing for the partition  $N_{A(BCD)}$ , its behavior in other partitions, such as  $N_{C(ABD)}$  and  $N_{D(ABC)}$ , is similar to that of the standard multipartite states like the  $GHZ_4$ . The identical decay patterns of  $N_{C(ABD)}$  and  $N_{D(ABC)}$  for both  $CL_4$  and  $GHZ_4$  states suggest that the exceptional topological robustness of the  $CL_4$  state is partition-specific. This means that the cluster state's topological protection is confined to certain correlations, offering complete preservation of entan-

lement only in specific partitions, while other partitions display behavior akin to conventional multipartite states. Thus, the  $CL_4$  state’s robustness is not universal but rather selectively protects particular bipartitions from thermal noise.

#### IV. CONCLUSIONS

In this work, we have systematically examined the properties of quantum entanglement for the tetrapartite  $CL_4$  state in the curved spacetime of a Schwarzschild black hole. We consider a four-party scenario consisting of Alice, Bob, Charlie, and David, where all observers start in an asymptotically flat spacetime region, except for David, who subsequently moves toward the event horizon of the black hole. Contrary to the prevailing view that Hawking radiation universally degrades quantum correlations, our results reveal a structured, partition-dependent hierarchy of resilience, with the  $CL_4$  state exhibiting unique and remarkable properties. A key finding of our study, within the single-mode approximation, is the exclusive phenomenon of “complete freezing of initially maximal entanglement” of the  $CL_4$  state in Schwarzschild spacetime. Quantified by negativity, the entanglement remains strictly maximal ( $N_{A(BCD)}^{CL_4} = 1$ ) for all values of the Hawking temperature, demonstrating perfect preservation and complete decoupling from the thermal fluctuations of the black hole. This stands in stark contrast to the monotonic degradation of entanglement observed in both bipartite states [1–5] and multipartite GHZ and W states [63–69]. This comparison highlights that the “complete freezing effect” is not a generic feature of all entangled states, but rather a distinctive characteristic of the  $CL_4$  state’s specific graph-theoretic structure, marking the first discovery of this unique phenomenon in curved spacetime. For the remaining bipartitions, a more nuanced picture emerges. The negativities  $N_{C(ABD)}$  and  $N_{D(ABC)}$  for both the  $CL_4$  and  $GHZ_4$  states exhibit identical decay trajectories, each approaching a non-zero plateau without sudden death. Across all three states, a consistent two-level hierarchy emerges: within each state,  $N_{C(ABD)} > N_{D(ABC)}$ , and across states, the  $W_4$  state consistently exhibits the lowest entanglement. These results suggest that while the stabilization of entanglement at large Hawking temperatures is a common feature of graph-based states, the magnitude of this stabilization depends on the specific structure of the entanglement.

From a theoretical perspective, within the single-mode approximation, previous studies have generally concluded that relativistic effects cause significant degradation of initially maximal entanglement in curved spacetime [1–10]. However, our findings challenge this traditional view,

marking the first discovery of the phenomenon of “complete freezing of initially maximal entanglement.” From a practical standpoint, our work identifies the  $CL_4$  state as a uniquely promising resource for quantum information processing, particularly in strong gravitational fields. Its ability to preserve either maximal or stable entanglement makes it an ideal candidate for relativistic quantum information tasks. Thus, this study not only advances our understanding of entanglement dynamics in curved spacetime but also provides a concrete pathway for developing robust quantum technologies that can transcend inertial limitations.

### Acknowledgments

This work is supported by the National Natural Science Foundation of China (12575056) and the Special Fund for Basic Scientific Research of Provincial Universities in Liaoning under grant NO. LS2024Q002.

---

- [1] W. Liu, C. Wen, J. Wang, Lorentz violation alleviates gravitationally induced entanglement degradation, *J. High Energy Phys.* **2025**, 184 (2025).
- [2] S. Sen, A. Mukherjee and S. Gangopadhyay, Entanglement degradation as a tool to detect signatures of modified gravity, *Phys. Rev. D* **109**, 046012 (2024).
- [3] I. Fuentes-Schuller and R. B. Mann, Alice falls into a black hole: Entanglement in non-inertial frames, *Phys. Rev. Lett.* **95**, 120404 (2005).
- [4] Q. Pan and J. Jing, Hawking radiation, entanglement, and teleportation in the background of an asymptotically flat static black hole, *Phys. Rev. D* **78**, 065015 (2008).
- [5] H. Wu and L. Chen, Orbital angular momentum entanglement in noninertial reference frame, *Phys. Rev. D* **107**, 065006 (2023).
- [6] S. M. Wu, X. W. Fan, R. D. Wang, H. Y. Wu, X. L. Huang and H. S. Zeng, Does Hawking effect always degrade fidelity of quantum teleportation in Schwarzschild spacetime?, *J. High Energy Phys.* **2023**, 232 (2023).
- [7] E. Martín-Martínez, L. J. Garay and J. León, Unveiling quantum entanglement degradation near a Schwarzschild black hole, *Phys. Rev. D* **82**, 064006 (2010).

- [8] P. M. Alsing, I. Fuentes-Schuller, R. B. Mann and T. E. Tessier, Entanglement of Dirac fields in non-inertial frames, *Phys. Rev. A* **74**, 032326 (2006).
- [9] W. M. Li, S. M. Wu, Bosonic and fermionic coherence of N-partite states in the background of a dilaton black hole, *J. High Energy Phys.* **2024**, 144 (2024).
- [10] M. M. Du, H. W. Li, S. T. Shen, X. J. Yan, X. Y. Li, L. Zhou, W. Zhong and Y. B. Sheng, Maximal steered coherence in the background of Schwarzschild space-time, *Eur. Phys. J. C* **84**, 450 (2024).
- [11] S. Elghaayda, A. Ali, S. Al-Kuwari and M. Mansour, Physically accessible and inaccessible quantum correlations of Dirac fields in Schwarzschild spacetime, *Phys. Lett. A* **525**, 129915 (2024).
- [12] J. K. Basak, D. Giataganas, S. Mondal and W. Y. Wen, Reflected entropy and Markov gap in noninertial frames, *Phys. Rev. D* **108**, 125009 (2023).
- [13] A. Ali, S. Al-Kuwari, M. Ghominejad, M. T. Rahim, D. Wang and S. Haddadi, Quantum characteristics near event horizons, *Phys. Rev. D* **110**, 064001 (2024).
- [14] C. Y. Liu, Z. W. Long and Q. L. He, Quantum coherence and quantum Fisher information of Dirac particles in curved spacetime under decoherence, *Phys. Lett. B* **857**, 138991 (2024).
- [15] T. Zhang, X. Wang and S. M. Fei, Hawking effect can generate physically inaccessible genuine tripartite nonlocality, *Eur. Phys. J. C* **83**, 607 (2023).
- [16] S. M. Wu, H. Y. Wu, Y. X. Wang, J. Wang, Gaussian tripartite steering in Schwarzschild black hole, *Phys. Lett. B* **865**, 139493 (2025).
- [17] G. Adesso, I. Fuentes-Schuller and M. Ericsson, Continuous variable entanglement sharing in non-inertial frames, *Phys. Rev. A* **76**, 062112 (2007).
- [18] S. M. Wu, X. W. Teng, W. M. Li, Y. X. Wang, J. Lu, Nonseparability of multipartite systems in dilaton black hole, *JCAP* **09**, 030 (2025).
- [19] G. W. Mi, X. Huang, S. M. Fei, T. Zhang, Quantumness near the Schwarzschild black hole based on W-state, *Ann. Phys. (Berlin)* **537**, e00397 (2025).
- [20] S. Harikrishnan, S. Jambulingam, P. P. Rohde and C. Radhakrishnan, Accessible and inaccessible quantum coherence in relativistic quantum systems, *Phys. Rev. A* **105**, 052403 (2022).
- [21] G. W. Mi, X. Huang, S. M. Fei, T. Zhang, Genuine four-partite Bell nonlocality in the curved space-time, *Eur. Phys. J. C* **85**, 354 (2025).
- [22] T. Y. Wang and D. Wang, Entropic uncertainty relations in Schwarzschild space-time, *Phys. Lett. B* **855**, 138876 (2024).
- [23] S. Bellucci, V. Kh. Kotanjyan, A. A. Saharian, Fermionic condensate and the mean energy-momentum

tensor in the Fulling-Rindler vacuum, *Phys. Rev. D* **108**, 085014 (2023).

[24] G. W. Mi, X. Huang, S. M. Fei, T. Zhang, Impact of the Hawking Effect on the fully entangled fraction of three-qubit states in Schwarzschild spacetime, *Ann. Phys. (Berlin)* **537**, 2400308 (2024).

[25] H. E. Camblong, A. Chakraborty, P. Lopez-Duque, C. R. Ordóñez, Entanglement degradation in causal diamonds, *Phys. Rev. D* **109**, 105003 (2024).

[26] L. J. Li, F. Ming, X. K. Song, L. Ye and D. Wang, Quantumness and entropic uncertainty in curved space-time, *Eur. Phys. J. C* **82**, 726 (2022).

[27] A. Belfiglio, O. Luongo, S. Mancini, Quantum entanglement in cosmology, *Phys. Rep.* **1146**, 1-47 (2025).

[28] X. Liu, W. Liu, Z. Liu, J. Wang, Harvesting correlations from BTZ black hole coupled to a Lorentz-violating vector field, *J. High Energy Phys.* **2025**, 94 (2025).

[29] Z. D. Wei, W. Han, Y. J. Zhang, Z. X. Man, Y. J. Xia, H. Fan, Effect of the gravitational redshift on the precision of phase estimation, *Phys. Rev. D* **111**, 026007 (2025).

[30] W. Izquierdo, J. Beltran, E. Arias, Enhancement of harvesting vacuum entanglement in Cosmic String Spacetime, *J. High Energy Phys.* **2025**, 49 (2025).

[31] Z. Liu, W. Liu, X. Liu, J. Wang, Wormhole-Induced correlation: A Link Between Two Universes, arXiv:2510.04005.

[32] S. M. Wu, C. X. Wang, D. D. Liu, X. L. Huang, H. S. Zeng, Would quantum coherence be increased by curvature effect in de Sitter space?, *J. High Energy Phys.* **2023**, 115 (2023).

[33] A. Chakraborty, L. Hackl, M. Zych, Entanglement harvesting in quantum superposed spacetime, *Phys. Rev. D* **111**, 104052 (2025).

[34] Z. Liu, R. Q. Yang, H. Fan, J. Wang, Simulation of the massless Dirac field in 1+1D curved spacetime, *Sci. China Phys. Mech. Astron.* **68**, 290411 (2025).

[35] S. M. Wu, R. D. Wang, X. L. Huang, Z. Wang, Does gravitational wave assist vacuum steering and Bell nonlocality?, *J. High Energy Phys.* **2024**, 155 (2024).

[36] Z. Liu, Y. Li, Z. Tian, J. Wang, Scrambling-Enhanced Quantum Battery Charging in Black Hole Analogues, *Adv. Sci.* e20281 (2025).

[37] X. Liu, Z. Tian, J. Jing, Entanglement dynamics in  $\kappa$ -deformed spacetime, *Sci. China Phys. Mech. Astron.* **67**, 100411 (2024).

[38] S. Barman, I. Chakraborty, S. Mukherjee, Signatures of gravitational wave memory in the radiative process of entangled quantum probes, *Phys. Rev. D* **111**, 025021 (2025).

[39] J. Foo, R. B. Mann, M. Zych, Entanglement amplification between superposed detectors in flat and curved spacetimes, *Phys. Rev. D* **103**, 065013 (2021).

[40] X. Liu, Z. Tian, J. Jing, Dissipation suppression for an Unruh-DeWitt battery with a reflecting boundary. *Sci. China Phys. Mech. Astron.* **68**, 100412 (2025).

[41] X. Liu, Z. Tian, J. Wang, J. Jing, Protecting quantum coherence of two-level atoms from vacuum fluctuations of electromagnetic field, *Ann. Phys.* **366**, 102-112 (2016).

[42] J. Foo, C. S. Arabaci, M. Zych, R. B. Mann, Quantum Signatures of Black Hole Mass Superpositions, *Phys. Rev. Lett.* **129**, 181301 (2022).

[43] J. Foo, C. S. Arabaci, M. Zych, R. B. Mann, Quantum superpositions of Minkowski spacetime, *Phys. Rev. D* **107**, 045014 (2023).

[44] M. M. Du, H. W. Li, Z. Tao, S. T. Shen, X. J. Yan, X. Y. Li, W. Zhong, Y. B. Sheng and L. Zhou, Basis-independent quantum coherence and its distribution under relativistic motion, *Eur. Phys. J. C* **84**, 838 (2024).

[45] Y. Ji, J. Zhang and H. Yu, Entanglement harvesting in cosmic string spacetime, *J. High Energy Phys.* **2024**, 161 (2024).

[46] Z. Liu, J. Zhang and H. Yu, Harvesting correlations from vacuum quantum fields in the presence of a reflecting boundary, *J. High Energy Phys.* **2023**, 184 (2023).

[47] Q. Liu, T. Liu, C. Wen, J. Wang, Optimal quantum strategy for locating Unruh channels, *Phys. Rev. A* **110**, 022428 (2024).

[48] Y. K. Zhang, L. J. Li, X. K. Song, L. Ye and D. Wang, Entropic uncertainty and quantum non-classicality of Unruh-Dewitt detectors in relativity, *Phys. Lett. B* **858**, 139063 (2024).

[49] S. H. Li, S. H. Shang, S. M. Wu, Does acceleration always degrade quantum entanglement for tetrapartite Unruh-DeWitt detectors?, *J. High Energy Phys.* **2025**, 214 (2025).

[50] T. Gonzalez-Raya, S. Pirandola and M. Sanz, Satellite-based entanglement distribution and quantum teleportation with continuous variables, *Commun. Phys.* **7**, 126 (2024).

[51] Y. Tang, W. Liu, Z. Liu, J. Wang, Can the latent signatures of quantum superposition be detected through correlation harvesting?, *J. High Energy Phys.* **2026**, 045 (2026).

[52] Y. Tang, W. Liu, J. Wang, Observational signature of Lorentz violation in acceleration radiation, *Eur. Phys. J. C* **85**, 1108 (2025).

[53] G. Ciliberto, S. Emig, N. Pavloff, M. Isoard, Violation of Bell inequalities in an analog black hole, *Phys. Rev. A* **109**, 063325 (2024).

[54] I. Agullo, A. Delhom, Á. Parra-López, Toward the observation of entangled pairs in BEC analog expanding universes, *Phys. Rev. D* **110**, 125023 (2024).

[55] A. A. Svidzinsky, M. O. Scully, W. Unruh, Minkowski vacuum entanglement and accelerated oscillator chains, *Phys. Rev. D* **111**, 045022 (2025).

[56] Q. Xiao, Y. Chen, T. Liu, Effects of Lorentz symmetry breaking on quantum coherence in an expanding universe, *Phys. Lett. B* **872**, 140133 (2026).

[57] T. Li, L. H. Liu, Cosmological complexity of the modified dispersion relation, *Phys. Lett. B* **854**, 138728 (2024).

[58] F. Ming, Z. Q. Xu, T. T. Lu, L. Dong, B. L. Fang, X. Hu, Y. Yu, H. Yang, D. Wang, Unveiling gravity-induced quantumness by three-measurement uncertainty relations, *Eur. Phys. J. C* **86**, 85 (2026).

[59] X. Liu, C. Wen, J. Wang, Quantum coherence of continuous variables in the black hole quantum atmosphere, *Phys. Lett. B* **868**, 139683 (2025).

[60] F. Shahbazi, S. Haseli, H. Dolatkhah, and S. Salimi, Entropic uncertainty relation in Garfinkle-Horowitz-Strominger dilation black hole, *JCAP* **10**, 047 (2020).

[61] P. K. Kumawat, S. Barman, B. R. Majhi, Equivalence in virtual transitions between uniformly accelerated and static atoms: from a bird's eye, *JCAP* **02**, 046 (2025).

[62] T. Li, L. H. Liu, Inflationary Krylov complexity, *J. High Energy Phys.* **2024**, 123 (2024).

[63] S. Xu, X. K. Song, J. D. Shi and L. Ye, How the Hawking effect affects multipartite entanglement of Dirac particles in the background of a Schwarzschild black hole, *Phys. Rev. D* **89**, 065022 (2014).

[64] A. J. Torres-Arenas, Q. Dong, G. H. Sun, W. C. Qiang and S. H. Dong, Entanglement measures of W-state in noninertial frames, *Phys. Lett. B* **789**, 93-105 (2019).

[65] R. Hamzehofi, M. Ashrafpour, D. Afshar, Genuine entanglement and quantum coherence of a multipartite W state in non-inertial frames, *Eur. Phys. J. Plus* **140**, 986 (2025).

[66] S. M. Wu and H. S. Zeng, Genuine tripartite nonlocality and entanglement in curved spacetime, *Eur. Phys. J. C* **82**, 4 (2022).

[67] M. R. Hwang, D. Park and E. Jung, Tripartite entanglement in a noninertial frame, *Phys. Rev. A* **83**, 012111 (2011).

[68] R. Hamzehofi, M. Ashrafpour, D. Afshar, Genuine Entanglement of a Multipartite GHZ State in Non-Inertial Frame, *Ann. Phys. (Berlin)* **537**, e00206 (2025).

[69] W. C. Qiang, G. H. Sun, Q. Dong and S. H. Dong, Genuine multipartite concurrence for entanglement of Dirac fields in noninertial frames, *Phys. Rev. A* **98**, 022320 (2018).

[70] H. J. Briegel and R. Raussendorf, Persistent Entanglement in Arrays of Interacting Particles, *Phys. Rev. Lett.* **86**, 910 (2001).

[71] V. S. Ferreira, G. Kim, A. Butler, H. Pichler, O. Painter, Deterministic generation of multidimensional photonic cluster states with a single quantum emitter, *Nat. Phys.* **20**, 865-870 (2024).

[72] C. Roh, G. Gwak, Y. D. Yoon, Y. S. Ra, Generation of three-dimensional cluster entangled state, *Nat. Photon.* **19**, 526-532 (2025).

[73] J. O'Sullivan, K. Reuer, A. Grigorev, et al., Deterministic generation of two-dimensional multi-photon cluster states, *Nat. Commun.* **16**, 5505 (2025).

[74] D. Cogan, Z. E. Su, O. Kenneth, D. Gershoni, Deterministic generation of indistinguishable photons in a cluster state, *Nat. Photon.* **17**, 324-329 (2023).

[75] D. Istrati, Y. Pilnyak, J. C. Loredo, et al., Sequential generation of linear cluster states from a single photon emitter, *Nat. Commun.* **11**, 5501 (2020).

[76] O. Pfister, Quantum cluster states engineered in three dimensions, *Nat. Photon.* **19**, 443-444 (2025).

[77] Y. Zhan and S. Sun, Deterministic Generation of Loss-Tolerant Photonic Cluster States with a Single Quantum Emitter, *Phys. Rev. Lett.* **125**, 223601 (2020).

[78] M. A. Nielsen, Cluster-state quantum computation, *Rep. Math. Phys.* **57**, 147-161 (2006).

[79] H. J. Briegel, D. E. Browne, W. Dür, R. Raussendorf, M. Van den Nest, Measurement-based quantum computation, *Nat. Phys.* **5**, 19-26 (2009).

[80] M. A. Nielsen, Optical quantum computation using cluster states, *Phys. Rev. Lett.* **93**, 040503 (2004).

[81] R. Raussendorf and H. J. Briegel, A One-Way Quantum Computer, *Phys. Rev. Lett.* **86**, 5188 (2001).

[82] R. F. Barros, G. B. Alves, O. Pfister, and A. Z. Khoury, Quantum-controlled cluster states, *Phys. Rev. A* **104**, 033713 (2021).

[83] J. Claes, J. E. Bourassa, S. Puri, Tailored cluster states with high threshold under biased noise, *npj Quantum Inf.* **9**, 9 (2023).

[84] R. Raussendorf, J. Harrington, Fault-tolerant quantum computation with high threshold in two dimensions, *Phys. Rev. Lett.* **98**, 190504 (2007).

[85] W. Dür and H. J. Briegel, Stability of macroscopic entanglement under decoherence, *Phys. Rev. Lett.* **92**, 180403 (2004).

[86] D. Garfinkle, G. T. Horowitz, and A. Strominger, Erratum: charged black holes in string theory, *Phys. Rev. D* **45**, 3888 (1992).

[87] Y. C. Ou and H. Fan, Monogamy inequality in terms of negativity for three-qubit states, *Phys. Rev. A*

### Appendix A: Quantum entanglement of the tetrapartite $GHZ$ state in Schwarzschild spacetime

In this appendix, we analyze the properties of the tetrapartite  $GHZ$  state within the same physical setup as for the  $CL_4$  state in Sec. III (see Fig.1). The initial tetrapartite  $GHZ$  state shared by the four observers (Alice, Bob, Charlie, David) in the asymptotically flat region is

$$|\Psi_{ABCD}^{GHZ_4}\rangle = \frac{1}{\sqrt{2}}(|0_A0_B0_C0_D\rangle + |1_A1_B1_C1_D\rangle). \quad (\text{A1})$$

To incorporate the Hawking effect on David's mode, we employ the Bogoliubov transformation in Eq.(11), which introduces an interior partner mode  $\bar{D}$  (anti-David). The expanded state becomes

$$|\Psi_{ABCD\bar{D}}^{GHZ_4}\rangle = \frac{1}{\sqrt{2}}\left(\frac{1}{\sqrt{e^{-\frac{\omega}{T}}+1}}|0\rangle_A|0\rangle_B|0\rangle_C|0\rangle_D|0\rangle_{\bar{D}} + \frac{1}{\sqrt{e^{\frac{\omega}{T}}+1}}|0\rangle_A|0\rangle_B|0\rangle_C|1\rangle_D|1\rangle_{\bar{D}} + |1\rangle_A|1\rangle_B|1\rangle_C|1\rangle_D|0\rangle_{\bar{D}}\right). \quad (\text{A2})$$

Tracing out the inaccessible mode  $\bar{D}$  yields the physical accessible reduced density matrix for the four exterior observers, which in the subspace spanned by  $|0000\rangle, |0001\rangle, |1111\rangle$  reads

$$\rho_{ABCD}^{GHZ_4} = \frac{1}{2} \begin{pmatrix} \frac{1}{e^{-\frac{\omega}{T}}+1} & 0 & \frac{1}{\sqrt{e^{-\frac{\omega}{T}}+1}} \\ 0 & \frac{1}{e^{\frac{\omega}{T}}+1} & 0 \\ \frac{1}{\sqrt{e^{-\frac{\omega}{T}}+1}} & 0 & 1 \end{pmatrix}. \quad (\text{A3})$$

We then evaluate the 1-3 tangle (negativity) described by the density matrix  $\rho_{ABCD}^{GHZ_4}$ . Taking the partial transpose with respect to modes  $A, C$  and  $D$ , we obtain the following matrices

$$\rho_{ABCD}^{GHZ_4(T_A)} = \frac{1}{2} \begin{pmatrix} \frac{1}{e^{-\frac{\omega}{T}}+1} & 0 & 0 & 0 & 0 \\ 0 & \frac{1}{e^{\frac{\omega}{T}}+1} & 0 & 0 & 0 \\ 0 & 0 & 0 & \frac{1}{\sqrt{e^{-\frac{\omega}{T}}+1}} & 0 \\ 0 & 0 & \frac{1}{\sqrt{e^{-\frac{\omega}{T}}+1}} & 0 & 0 \\ 0 & 0 & 0 & 0 & 1 \end{pmatrix}, \quad (\text{A4})$$

$$\rho_{ABCD}^{GHZ_4(T_C)} = \frac{1}{2} \begin{pmatrix} \frac{1}{e^{-\frac{\omega}{T}}+1} & 0 & 0 & 0 & 0 \\ 0 & \frac{1}{e^{-\frac{\omega}{T}}+1} & 0 & 0 & 0 \\ 0 & 0 & 0 & \frac{1}{\sqrt{e^{-\frac{\omega}{T}}+1}} & 0 \\ 0 & 0 & \frac{1}{\sqrt{e^{-\frac{\omega}{T}}+1}} & 0 & 0 \\ 0 & 0 & 0 & 0 & 1 \end{pmatrix}, \quad (A5)$$

$$\rho_{ABCD}^{GHZ_4(T_D)} = \frac{1}{2} \begin{pmatrix} \frac{1}{e^{-\frac{\omega}{T}}+1} & 0 & 0 & 0 \\ 0 & \frac{1}{e^{-\frac{\omega}{T}}+1} & \frac{1}{\sqrt{e^{-\frac{\omega}{T}}+1}} & 0 \\ 0 & \frac{1}{\sqrt{e^{-\frac{\omega}{T}}+1}} & 0 & 0 \\ 0 & 0 & 0 & 1 \end{pmatrix}, \quad (A6)$$

where  $\rho_{ABCD}^{GHZ_4(T_A)}$  is expressed in the ordered basis  $|0000\rangle, |0001\rangle, |0111\rangle, |1000\rangle, |1111\rangle$ ;  $\rho_{ABCD}^{GHZ_4(T_C)}$  in  $|0000\rangle, |0001\rangle, |0010\rangle, |1101\rangle, |1111\rangle$ ; and  $\rho_{ABCD}^{GHZ_4(T_D)}$  in  $|0000\rangle, |0001\rangle, |1110\rangle, |1111\rangle$ . By employing Eq.(17), the corresponding negativities are

$$N_{A(BCD)}^{GHZ_4} = N_{C(ABD)}^{GHZ_4} = \max \left\{ 0, \frac{1}{\sqrt{1 + e^{-\frac{\omega}{T}}}} \right\}, \quad (A7)$$

$$N_{D(ABC)}^{GHZ_4} = \max \left\{ 0, \frac{1}{2} \left( \sqrt{\frac{4}{1 + e^{-\frac{\omega}{T}}} + \frac{1}{(1 + e^{\frac{\omega}{T}})^2}} - \frac{1}{1 + e^{\frac{\omega}{T}}} \right) \right\}. \quad (A8)$$

A key observation is that  $N_{C(ABD)}^{GHZ_4}$  and  $N_{D(ABC)}^{GHZ_4}$  are mathematically identical to the corresponding results for the  $CL_4$  state [Eqs.(22) and (23)]. This equivalence explains the coincident decay curves of the  $CL_4$  and  $GHZ_4$  states in Fig.3.

## Appendix B: Quantum entanglement of the tetrapartite $W$ state in Schwarzschild spacetime

The initial tetrapartite  $W$  state in the asymptotically flat region is

$$|\Psi_{ABCD}^{W_4}\rangle = \frac{1}{2}(|0_A 0_B 0_C 1_D\rangle + |0_A 0_B 1_C 0_D\rangle + |0_A 1_B 0_C 0_D\rangle + |1_A 0_B 0_C 0_D\rangle). \quad (B1)$$

Following the same procedure as for the  $CL_4$  and  $GHZ_4$  states, we apply the Bogoliubov transformation in Eq.(11) to David's mode, which gives the expanded state

$$\begin{aligned}
|\Psi_{ABCD\bar{D}}^{W_4}\rangle = & \frac{1}{2\sqrt{e^{-\frac{\omega}{T}}+1}}(|0\rangle_A|0\rangle_B|1\rangle_C|0\rangle_D|0\rangle_{\bar{D}} + |0\rangle_A|1\rangle_B|0\rangle_C|0\rangle_D|0\rangle_{\bar{D}} \\
& + |1\rangle_A|0\rangle_B|0\rangle_C|0\rangle_D|0\rangle_{\bar{D}}) + \frac{1}{2\sqrt{e^{\frac{\omega}{T}}+1}}(|0\rangle_A|0\rangle_B|1\rangle_C|1\rangle_D|1\rangle_{\bar{D}} \\
& + |0\rangle_A|1\rangle_B|0\rangle_C|1\rangle_D|1\rangle_{\bar{D}} + |1\rangle_A|0\rangle_B|0\rangle_C|1\rangle_D|1\rangle_{\bar{D}}) \\
& + \frac{1}{2}|0\rangle_A|0\rangle_B|0\rangle_C|1\rangle_D|0\rangle_{\bar{D}}. \tag{B2}
\end{aligned}$$

Tracing out  $\bar{D}$  yields the reduced density matrix for the four exterior observers. In the ordered basis  $|0001\rangle, |0010\rangle, |0011\rangle, |0100\rangle, |0101\rangle, |1000\rangle, |1001\rangle$ , the matrix reads

$$\rho_{ABCD}^{W_4} = \frac{1}{4} \begin{pmatrix} 1 & \frac{1}{\sqrt{e^{-\frac{\omega}{T}}+1}} & 0 & \frac{1}{\sqrt{e^{-\frac{\omega}{T}}+1}} & 0 & \frac{1}{\sqrt{e^{-\frac{\omega}{T}}+1}} & 0 \\ \frac{1}{\sqrt{e^{-\frac{\omega}{T}}+1}} & \frac{1}{e^{-\frac{\omega}{T}}+1} & 0 & \frac{1}{e^{-\frac{\omega}{T}}+1} & 0 & \frac{1}{e^{-\frac{\omega}{T}}+1} & 0 \\ 0 & 0 & \frac{1}{e^{\frac{\omega}{T}}+1} & 0 & \frac{1}{e^{\frac{\omega}{T}}+1} & 0 & \frac{1}{e^{\frac{\omega}{T}}+1} \\ \frac{1}{\sqrt{e^{-\frac{\omega}{T}}+1}} & \frac{1}{e^{-\frac{\omega}{T}}+1} & 0 & \frac{1}{e^{-\frac{\omega}{T}}+1} & 0 & \frac{1}{e^{-\frac{\omega}{T}}+1} & 0 \\ 0 & 0 & \frac{1}{e^{\frac{\omega}{T}}+1} & 0 & \frac{1}{e^{\frac{\omega}{T}}+1} & 0 & \frac{1}{e^{\frac{\omega}{T}}+1} \\ \frac{1}{\sqrt{e^{-\frac{\omega}{T}}+1}} & \frac{1}{e^{-\frac{\omega}{T}}+1} & 0 & \frac{1}{e^{-\frac{\omega}{T}}+1} & 0 & \frac{1}{e^{-\frac{\omega}{T}}+1} & 0 \\ 0 & 0 & \frac{1}{e^{\frac{\omega}{T}}+1} & 0 & \frac{1}{e^{\frac{\omega}{T}}+1} & 0 & \frac{1}{e^{\frac{\omega}{T}}+1} \end{pmatrix}. \tag{B3}$$

Next we compute the  $1 - 3$  tangle for the tetrapartite  $W$  state by performing the partial transposition with respect to modes  $A, C$  and  $D$ . The resulting matrices can be expressed as

$$\rho_{ABCD}^{W_4(T_A)} = \frac{1}{4} \begin{pmatrix} 0 & 0 & 0 & 0 & 0 & 0 & 0 & \frac{1}{\sqrt{e^{-\frac{\omega}{T}}+1}} & \frac{1}{e^{-\frac{\omega}{T}}+1} & 0 & \frac{1}{e^{-\frac{\omega}{T}}+1} & 0 \\ 0 & 1 & \frac{1}{\sqrt{e^{-\frac{\omega}{T}}+1}} & 0 & \frac{1}{\sqrt{e^{-\frac{\omega}{T}}+1}} & 0 & 0 & 0 & 0 & \frac{1}{e^{\frac{\omega}{T}}+1} & 0 & \frac{1}{e^{\frac{\omega}{T}}+1} \\ 0 & \frac{1}{\sqrt{e^{-\frac{\omega}{T}}+1}} & \frac{1}{e^{-\frac{\omega}{T}}+1} & 0 & \frac{1}{e^{-\frac{\omega}{T}}+1} & 0 & 0 & 0 & 0 & 0 & 0 & 0 \\ 0 & 0 & 0 & \frac{1}{e^{\frac{\omega}{T}}+1} & 0 & \frac{1}{e^{\frac{\omega}{T}}+1} & 0 & 0 & 0 & 0 & 0 & 0 \\ 0 & \frac{1}{\sqrt{e^{-\frac{\omega}{T}}+1}} & \frac{1}{e^{-\frac{\omega}{T}}+1} & 0 & \frac{1}{e^{-\frac{\omega}{T}}+1} & 0 & 0 & 0 & 0 & 0 & 0 & 0 \\ 0 & 0 & 0 & \frac{1}{e^{\frac{\omega}{T}}+1} & 0 & \frac{1}{e^{\frac{\omega}{T}}+1} & 0 & 0 & 0 & 0 & 0 & 0 \\ 0 & 0 & 0 & \frac{1}{e^{\frac{\omega}{T}}+1} & 0 & \frac{1}{e^{\frac{\omega}{T}}+1} & 0 & 0 & 0 & 0 & 0 & 0 \\ \frac{1}{\sqrt{e^{-\frac{\omega}{T}}+1}} & 0 & 0 & 0 & 0 & 0 & 0 & \frac{1}{e^{\frac{\omega}{T}}+1} & 0 & 0 & 0 & 0 \\ \frac{1}{e^{-\frac{\omega}{T}}+1} & 0 & 0 & 0 & 0 & 0 & 0 & 0 & 0 & 0 & 0 & 0 \\ 0 & \frac{1}{e^{\frac{\omega}{T}}+1} & 0 & 0 & 0 & 0 & 0 & 0 & 0 & 0 & 0 & 0 \\ \frac{1}{e^{-\frac{\omega}{T}}+1} & 0 & 0 & 0 & 0 & 0 & 0 & 0 & 0 & 0 & 0 & 0 \\ 0 & \frac{1}{e^{\frac{\omega}{T}}+1} & 0 & 0 & 0 & 0 & 0 & 0 & 0 & 0 & 0 & 0 \end{pmatrix} \tag{B4}$$

$$\rho_{ABCD}^{W_4(T_C)} = \frac{1}{4} \begin{pmatrix} 0 & 0 & 0 & \frac{1}{\sqrt{e^{-\frac{\omega}{T}}+1}} & 0 & 0 & \frac{1}{e^{-\frac{\omega}{T}}+1} & 0 & 0 & 0 & \frac{1}{e^{-\frac{\omega}{T}}+1} & 0 \\ 0 & 1 & 0 & 0 & \frac{1}{\sqrt{e^{-\frac{\omega}{T}}+1}} & 0 & 0 & \frac{1}{e^{-\frac{\omega}{T}}+1} & \frac{1}{\sqrt{e^{-\frac{\omega}{T}}+1}} & 0 & 0 & \frac{1}{e^{-\frac{\omega}{T}}+1} \\ 0 & 0 & \frac{1}{e^{-\frac{\omega}{T}}+1} & 0 & 0 & 0 & 0 & 0 & 0 & 0 & 0 & 0 \\ \frac{1}{\sqrt{e^{-\frac{\omega}{T}}+1}} & 0 & 0 & \frac{1}{e^{-\frac{\omega}{T}}+1} & 0 & 0 & 0 & 0 & 0 & 0 & 0 & 0 \\ 0 & \frac{1}{\sqrt{e^{-\frac{\omega}{T}}+1}} & 0 & 0 & \frac{1}{e^{-\frac{\omega}{T}}+1} & 0 & 0 & 0 & \frac{1}{e^{-\frac{\omega}{T}}+1} & 0 & 0 & 0 \\ \frac{1}{e^{-\frac{\omega}{T}}+1} & 0 & 0 & 0 & 0 & \frac{1}{e^{-\frac{\omega}{T}}+1} & 0 & 0 & 0 & \frac{1}{e^{-\frac{\omega}{T}}+1} & 0 & 0 \\ 0 & \frac{1}{e^{-\frac{\omega}{T}}+1} & 0 & 0 & 0 & 0 & 0 & 0 & 0 & 0 & 0 & 0 \\ 0 & \frac{1}{\sqrt{e^{-\frac{\omega}{T}}+1}} & 0 & 0 & \frac{1}{e^{-\frac{\omega}{T}}+1} & 0 & 0 & 0 & \frac{1}{e^{-\frac{\omega}{T}}+1} & 0 & 0 & 0 \\ 0 & 0 & 0 & 0 & 0 & \frac{1}{e^{-\frac{\omega}{T}}+1} & 0 & 0 & 0 & \frac{1}{e^{-\frac{\omega}{T}}+1} & 0 & 0 \\ \frac{1}{e^{-\frac{\omega}{T}}+1} & 0 & 0 & 0 & 0 & 0 & 0 & 0 & 0 & 0 & 0 & 0 \\ 0 & \frac{1}{e^{-\frac{\omega}{T}}+1} & 0 & 0 & 0 & 0 & 0 & 0 & 0 & 0 & 0 & 0 \end{pmatrix} \quad (B5)$$

$$\rho_{ABCD}^{W_4(T_D)} = \frac{1}{4} \begin{pmatrix} 0 & 0 & 0 & \frac{1}{\sqrt{e^{-\frac{\omega}{T}}+1}} & 0 & \frac{1}{\sqrt{e^{-\frac{\omega}{T}}+1}} & 0 & \frac{1}{\sqrt{e^{-\frac{\omega}{T}}+1}} \\ 0 & 1 & 0 & 0 & 0 & 0 & 0 & 0 \\ 0 & 0 & \frac{1}{e^{-\frac{\omega}{T}}+1} & 0 & \frac{1}{e^{-\frac{\omega}{T}}+1} & 0 & \frac{1}{e^{-\frac{\omega}{T}}+1} & 0 \\ \frac{1}{\sqrt{e^{-\frac{\omega}{T}}+1}} & 0 & 0 & \frac{1}{e^{-\frac{\omega}{T}}+1} & 0 & \frac{1}{e^{-\frac{\omega}{T}}+1} & 0 & \frac{1}{e^{-\frac{\omega}{T}}+1} \\ 0 & 0 & \frac{1}{e^{-\frac{\omega}{T}}+1} & 0 & \frac{1}{e^{-\frac{\omega}{T}}+1} & 0 & \frac{1}{e^{-\frac{\omega}{T}}+1} & 0 \\ \frac{1}{\sqrt{e^{-\frac{\omega}{T}}+1}} & 0 & 0 & \frac{1}{e^{-\frac{\omega}{T}}+1} & 0 & \frac{1}{e^{-\frac{\omega}{T}}+1} & 0 & \frac{1}{e^{-\frac{\omega}{T}}+1} \\ 0 & 0 & \frac{1}{e^{-\frac{\omega}{T}}+1} & 0 & \frac{1}{e^{-\frac{\omega}{T}}+1} & 0 & \frac{1}{e^{-\frac{\omega}{T}}+1} & 0 \\ \frac{1}{\sqrt{e^{-\frac{\omega}{T}}+1}} & 0 & 0 & \frac{1}{e^{-\frac{\omega}{T}}+1} & 0 & \frac{1}{e^{-\frac{\omega}{T}}+1} & 0 & \frac{1}{e^{-\frac{\omega}{T}}+1} \end{pmatrix}, \quad (B6)$$

where  $\rho_{ABCD}^{W_4(T_A)}$  is expressed in the ordered basis  $|0000\rangle, |0001\rangle, |0010\rangle, |0011\rangle, |0100\rangle, |0101\rangle, |1000\rangle, |1001\rangle, |1010\rangle, |1011\rangle, |1100\rangle, |1101\rangle$ ;  $\rho_{ABCD}^{W_4(T_C)}$  in  $|0000\rangle, |0001\rangle, |0010\rangle, |0011\rangle, |0100\rangle, |0101\rangle, |0110\rangle, |0111\rangle, |1000\rangle, |1001\rangle, |1010\rangle, |1011\rangle$ ; and  $\rho_{ABCD}^{W_4(T_D)}$  in  $|0000\rangle, |0001\rangle, |0010\rangle, |0011\rangle, |0100\rangle, |0101\rangle, |1000\rangle, |1001\rangle$ . Applying Eq.(17) to these matrices yields the corresponding negativities. Due to the complexity of the expressions for  $N_{A(BCD)}^{W_4}$  and  $N_{C(ABD)}^{W_4}$ , we refrain from presenting them explicitly here. For the negativity  $N_{D(ABC)}^{W_4}$ , we obtain the following compact expression

$$N_{D(ABC)}^{W_4} = \max \left\{ 0, \frac{1}{4} \left( \sqrt{\frac{12}{1+e^{-\frac{\omega}{T}}}} + \frac{9}{(1+e^{\frac{\omega}{T}})^2} - \frac{3}{1+e^{\frac{\omega}{T}}} \right) \right\}. \quad (B7)$$